GuideAndTrack: A Novel Guidance and Localization Method by a Handheld UHF-RFID Reader

Spyros Megalou, Ioanna S. Ellina, Evangelos Kouros, Aristidis Raptopoulos Chatzistefanou, Nikolaos Fachantidis, Traianos V. Yioultsis, *Member, IEEE,* and Antonis G. Dimitriou, *Senior, IEEE*

***Abstract*—In this paper we present GuideAndTrack; a prototype method for guiding a user to any RFID-tagged target. The user is equipped with a handheld RFID reader, which measures the phase of RFID tags placed at known positions in the map. Motion of the user is captured by estimating the Rate Of Change (ROC) of the collected phase measurements along discrete time-slots; i.e. null rate implies zero radial vector with respect to the corresponding tag, while negative/positive rates signify approaching towards or moving away from the corresponding tag respectively. The phase ROC represents an advantageous metric for accurate localization, since it can be easily measured in any given time-slot and does not necessitates knowledge of the prior state of the reader-to-tag link. The proposed method, initially estimates the direction of motion of the user, by sorting the estimated phase-ROCs from the surrounding tags during one's translational motion, guiding one to the desired target. Then, the position of the user is accurately estimated by feeding the estimated phase-ROCs in a particle filter. The proposed method has been experimentally verified in two cases; one by deploying a robot, in order to acquire the ground truth of the moving "user" and another case, where a human held a portable RFID reader. In all cases, the method performed well, guiding the user to the desired target, while estimating one's pose accurately. Characteristic results and comparison with prior art are presented herein.**

***Index Terms*—RFID, tracking, particle filter, phase, portable reader.**

I. Introduction

NUMEROUS aspects of our daily life are starting to change as a result of the Fourth Industrial Revolution. The ongoing automation and optimization of traditional manufacturing, product processing, and industrial operations and services are significantly aided by Radio Frequency Identification (RFID) technology. Innovative RFID applications are beginning to arise in a variety of end-user applications as RFID tags and readers become more widely available and more reasonably priced with the aim of delivering services like assisted living or better and more personalised user experiences.

In this paper, we introduce GuideAndTrack (GAT) an innovative RFID-based system for directing a user to a specific target in an area. The idea has emerged as an applied solution to provide guided tours in a museum exploiting the installed RFID technology. Prior art on museum indoor tracking is mostly focused on crowd behavior sensing and retail analytics by tracking visitors' positions [1]–[3].

In this work the proposed method ensures both guidance and tracking. The user carries a prototype handheld reader manufactured with Commercial Off The Shelf (COTS) hardware, capable of measuring the phase from tags around it. RFID tags positioned at known locations (e.g. exhibits, specific showcases etc.) are interrogated by the reader, providing phase and power information. By exploiting the phase data of the backscattered signal at the reader, we develop a novel method that ensures user guidance to any specific RFID tag.

The portable reader guides the user by calculating the rate of change (ROC) of phase measurements. When the reader is approaching a tag, the phase of the tag's backscattered signal is decreasing in respect to time. The rate of this decrease is higher when the reader is moving towards the tag and its trajectory coincides with the direct line of minimum distance between the tag and the reader. This property is exploited to determine the user's motion direction. To estimate the reader's position and guide the user, until reaching the target tag, a particle filter algorithm is deployed. GuideAndTrack updates the filters and improves location prediction, based on sequential phase measurements received from the surrounding tags.

Prior art on target localization and guidance with RFID technology involves using a variety of signal information gleaned from the tags' backscattered signal. One or more stationary RFID tags represent the intended target. The main measuring tools are an RFID reader and a variety of antennas. The Received Signal Power or Received Signal Strength Indicator (RSSI) is used in [4] - [6]. In [4] and [5], a motorized cart with numerous antennas is maneuvered around a space containing reference RFID tags dispersed at known positions. Using the RSSI readings from the reference tags, the positions of the target and the cart are both determined. In [6] a robot carries

Manuscript received Mar 4, 2023.

This research has been co-financed by the European Union and Greek national funds through the Operational Program Competitiveness, Entrepreneurship and Innovation, under the call RESEARCH – CREATE – INNOVATE (project code:T2EDK-02000.)

The implementation of the doctoral thesis was co-financed by Greece and the European Union (European Social Fund-ESF) through the Operational Programme "Human Resources Development, Education and Lifelong Learning" in the context of the Act "Enhancing Human Resources Research Potential by undertaking a Doctoral Research" Sub-action 2: IKY Scholarship Programme for PhD candidates in the Greek Universities

Nikolaos Fachantidis is with the Dept. of Educational and Social Policy, University of Macedonia, Thessaloniki, Greece (e-mail: nfachantidis@uom.edu.gr).

All other authors are with the School of Electrical and Computer Engineering, Aristotle University of Thessaloniki, Thessaloniki, Greece (e-mail: antodimi@ece.auth.gr).

the measuring apparatus. It moves autonomously, creates a map of the area, and calculates its location. The target's location is estimated using a Bayesian filter and RSSI readings.

However, received signal strength is not a trustworthy indicator because it is heavily affected by unpredictable factors such as multipath and shadowing, limiting positioning accuracy. Phase of Arrival (POA) measurements measurements on the other hand, can be used in many ways achieving higher estimation accuracy. In [7]–[11] wrapped phase measurements from one or multiple antennas on a robot capable of performing Simultaneous Localization And Mapping (SLAM) are used to locate the target tag. In contrast to the current problem, all these methods estimate the position of the reader using SLAM and focus only on locating stationary tags in respect to reader's/robot's position.

Other methods [12], [13] need multiple frequency channels to tackle the effect of multipath and locate the target. However, most multi-frequency algorithms were developed under US standards, which enable Gen 2 UHF RFID devices with increased bandwidth, compared to the bandwidth-restrictions applied in Europe.

Fusion of RFID measurements and other sensors (e.g. IMU, odometry etc.) is introduced in [14]–[16]. In [14], a portable device instructs the user to take specific actions while RFID reader and IMU measurements are gathered. The suggested approach estimates the distance and angle of a desired RFID tag for the user but can extract only a rough estimation of the followed trajectory. The approach described in [16] by the authors involves utilizing an Extended Kalman Filter (EKF) to combine POA and odometry information in order to determine the bearing and distance of the target tag from the robot's present attitude. As the robot makes progress toward the intended destination, updated measurements help to refine the estimation. A portable measuring system is used in [15]. IMU data are used to determine the location of the human operator, and phase measurements are gathered to find targets.

The rate of change of phase has been used in some interesting ways in [17], [18]. In [17], the authors sought to combine acceleration data from an IMU with the second derivative of phase measurements. They manage to reach the target's location in multipath environments but do not present a way of knowing the position of the handheld reader.

In [18] tag's mobility is exploited to build a virtual antenna array by using readings from a few physical antennas over a time window. The tag's starting position is presumed on a grid in the monitored region. The target's velocity is estimated for each grid place by analyzing the discrepancies between successive phase measurements and radial velocity vectors. A Differential Augmented Hologram (DAH) is suggested to enable rapid and accurate tracking of mobile RFID tags at a known track (e.g. conveyor belt). The tag's trajectory in an unknown track is extracted by pinpointing the initial position of the tag and then recovering the trajectory using a chain of radial velocity vectors. In multipath rich environments noise is added on the chain of radial velocities making all the possible trajectories "look" similar. This way the process of pinpointing the starting point and extracting the closest trajectory to the real one becomes challenging increasing the mean error of the estimation. In addition Tagoram considers a calculations' grid, posing a trade-off between accuracy and execution-speed.

Other methods can also be used for guiding and navigation in addition to RFID technology. A research on indoor positioning technology is carried out in [19] and a survey of indoor assistance systems for visually impaired people is presented in [25]. Vision-based systems, ultrasonic localization, various RF technologies like Wi-Fi and bluetooth, and inertial navigation systems are only a few of the techniques discussed. In [20], a system comprised of a camera, a Wi-Fi sensor, and an IMU is used to map the surroundings in 3D and then find the user inside that map. In [21]–[23], a map is created using a camera and the inertial sensors of a smartphone or tablet, and an Augmented Reality (AR) application guides the user to the target destination by giving visual or auditory guidance. Authors in [24] use a depth camera while a panoramic visual odometry system is exploited in [26] to obtain image information, including the entire ceiling and doors. Low-cost Bluetooth beacons are scattered in indoor areas of interest in [27] estimating the human target's position by exploiting the RSSI detected through a smart phone.

In this paper we estimate the Rate of Change (ROC) of phase to explore a different problem where a moving antenna aims a stationary tagged target, while the antenna's position is tracked in real-time by phase measurements collected from fixed RFID tags at known positions. By exploiting particle filters and estimating the position of the moving target in successive time instants the algorithm maintains a low mean error for all experiments even in multipath rich environments. A handheld reader provides audio and visual instructions to guide the user to the predefined target while self locating itself in the monitored area.

In comparison to previous works, the suggested technique uses inexpensive COTS equipment to estimate pose (position and direction) accurately. The technique determines 1) the direction towards where the reader/human is moving and 2) the reader's location in the area. The concept has been developed as a practical approach to offering guided walks in a museum taking advantage of the installed RFID technology (i.e. tagged exhibits). Prior art on visitors' tracking primarily focuses on monitoring a human's position using antennas in the perimeter of the search region to extract retail analytics. In most cases, such techniques do not include direction estimation and neither identify the target's orientation nor compute it as a conjecture based on the target's movements. In this paper, we propose a novel technique for guidance and tracking. The method is real-time and integrated in a prototype portable reader. Because of this, the technique can be applied to other fields like retail stores, libraries and warehouses, where the operator searches and is guided towards a specific item; such process is currently integrated in some handheld readers in the market, by exploiting only the received power of the selected tag, where the reader "beeps" louder according to the measured power. The proposed method provides direction and position to the operator. The following can be used to summarize GuideAndTrack's contribution:

- The estimated ROC of phase measurements from tags placed in known positions is used as a spatial indicator.

- Since localization and tracking occur in successive time periods, phase-unwrapping of the entire measurements is not necessary. Each time-period is treated separately and independently from all other time-periods. This ensures robustness of the proposed method, even when phase-data from a given tag become unavailable, due to multipath. Phase measurements are unwrapped for each time-period only to estimate the ROC of phase along the selected time-window.
- The phase-ROC of interrogated tags in each step (time window) can be calculated even with partial/fragmentary sequences of phase.
- The suggested portable device exploits COTS components and may be carried by a human operator.
- The device collects all the necessary data, which are then processed locally to produce **real-time** localization and tracking results.
- Localization and tracking is independent from guidance; the user's pose is tracked for any motion.
- The proposed method could be applied in a variety of scenarios, including possible guidance to blind people.

II. GuideAndTrack - Theoretical Analysis

Consider the scenario where a human is walking in an unknown space and needs to be guided to an RFID tag attached on a specific target. More RFID tags are positioned at known locations in the space of interest. The person is holding a portable RFID reader that will help him throughout the process. The handheld reader collects phase and RSSI measurements associated with each RFID tag and and uses audio and visual feedback to lead the user to the target tag.

GuideAndTrack can be decomposed in two separate procedures. The direction estimation and the location estimation. To determine the user's direction of motion, the phase-ROCs of all tags are calculated. The tag presenting the minimum rate is the tag that the user is moving towards to. After calculating the direction of the user the portable reader gives corresponding instructions (e.g. turn slightly left/right, keep walking forward, etc). The direction estimation procedure is presented in further detail in II-B.

To notify the user that the target has been met, or guide a potential blind user around known obstacles of the map, the reader's position must be estimated in real time. Initially, a collection of particles is randomly distributed around the search space region. Each particle has a likelihood weight which is updated based on the comparison of theoretical and measured phase-ROCs received from the surrounding tags. The target's position is estimated using the weighted mean of the particle states. The location estimation algorithm based on particle filters is presented in II-C.

A. Measured Data

Consider a person carrying a portable reader and RFID tags fixed at known locations as shown in Fig. 1. The positions of the moving reader's antenna at discrete timestamps j are denoted by $\mathbf{A}_{ant,j} = [x_{ant,j}, y_{ant,j}]$ and the corresponding

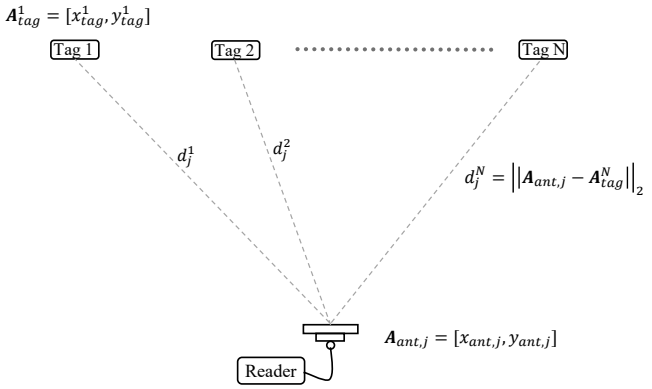

Fig. 1. A portable reader interrogates RFID tags at time instant t_j.

fixed position of the i_{th} tag is $\mathbf{A}^i_{tag} = [x^i_{tag}, y^i_{tag}]$. The distance between the antenna and the i_{th} tag at time j is:

$$||\mathbf{A}_{ant,j} - \mathbf{A}^i_{tag}||_2 = \sqrt{(x_{ant,j} - x^i_{tag})^2 + (y_{ant,j} - y^i_{tag})^2}, \quad (1)$$

The corresponding wrapped phase measurements are [28]:

$$\phi^i_j = (\phi^i_{prop,j} + \phi^i_o + \phi^i_{noise,j} + \phi^i_{mult,j}) mod(2\pi), \quad (2)$$

$$\phi^i_{noise,j} \sim \mathcal{N}(0, \sigma^2_{phase}), \quad (3)$$

$$\phi^i_{mult,j} = \tan^{-1}\left(\frac{Asin\theta}{1 + Acos\theta}\right), \quad (4)$$

where ϕ^i_o is the phase offset of the i_{th} tag, $\phi^i_{noise,j}$ is the measurement's noise and $\phi^i_{mult,j}$ is introduced to account for multipath. The propagation phase term $\phi^i_{prop,j}$ corresponds to the phase due to the round trip distance $2d^i_j$ between the reader at time j and the i_{th} tag, given by:

$$\phi^i_{prop,j} = \frac{2\pi}{\lambda} 2d^i_j, \quad (5)$$

where $d^i_j = ||\mathbf{A}_{ant,j} - \mathbf{A}^i_{tag}||_2$, given in (1).

The phase measured at the receiver can be interpreted as the resultant vector sum of two vectors: the direct Line-Of-Sight (LOS) vector of magnitude A_{LoS} and phase θ_{LoS} and the phase sum of all other contributions (reflected, scattered, etc.), referred herein as Non-Line-Of-Sight (NLOS) of magnitude A_{NLoS} and phase θ_{NLoS}. Typically, all other contributions are of smaller magnitude than the direct ray, as they have suffered multiple interactions with the environment, e.g. reflections, and have travelled a greater distance; i.e. $A_{NLoS} \leq A_{LoS}$. The two vectors are shown in Fig. 2. The phase of the NLOS vector is arbitrary with respect to the phase of the LOS component and can be considered uniformly distributed in $[0, 2\pi)$. Using vector analysis, and substituting $A = \frac{A_{NLoS}}{A_{LoS}}$ and $\theta = \theta_{NLoS} - \theta_{LoS}$ the resultant phase of the vector summation of the two components is given by (4). For a given amplitude ratio $A = \alpha$, the phase ϕ_{mult} is a random variable with probability density function:

$$f_\phi(\phi_{mult}|A = \alpha) = \frac{1}{\pi\sqrt{\alpha^2 + (\alpha^2 - 1)\tan^2\phi_{mult}}} \quad (6)$$

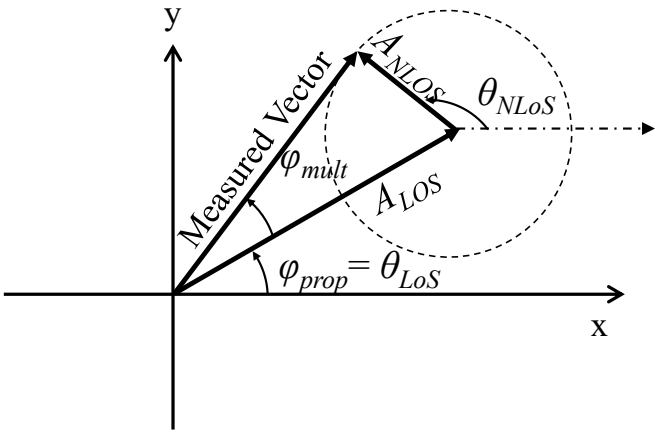

Fig. 2. Vector representation of the received signal due to multipath.

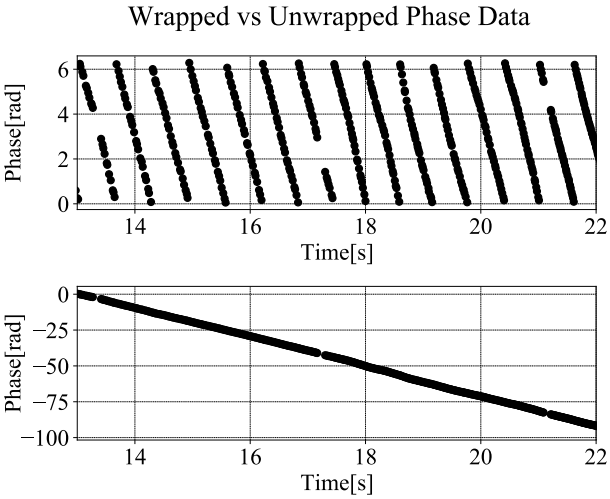

Fig. 3. Wrapped phase measurements in [0, 2π) collected from a reader moving towards a tag are presented at the top plot. The bottom plot shows the same measurements, after unwrapping.

and cumulative distribution function:

$$F_{\phi}(\phi_{mult}|A=\alpha) = \frac{2}{\pi}\tan^{-1}\left(\frac{\sqrt{2}\sin\phi_{mult}}{\sqrt{-1+2\alpha^2+\cos 2\phi_{mult}}}\right) \tag{7}$$

The effect of multipath, analyzed above, will be included in the simulation-results and will be further discussed in the measurements' section.

Next, let's consider a multipath free environment. For a selected period of time t sequential phase measurements are collected from all tags. For each tag the phase measurements have to be unwrapped, to calculate the corresponding ROC. In Fig. 3 wrapped and unwrapped phase measurements are shown. After unwrapping, phase ϕ_j^i is given by:

$$\phi_j^i = \phi_{prop,j}^i + \phi_o^i + \phi_{noise,j}^i \tag{8}$$

To overcome the influence of phase noise a second degree Savitzky–Golay filter is applied to smooth the data and mitigate the phase-deviations. The red line in Fig. 4 represents the phase data after filtering. This allows us to remove the $\phi_{noise,j}^i$ factor from (8). Let $d\phi_j^i$ denote the difference of

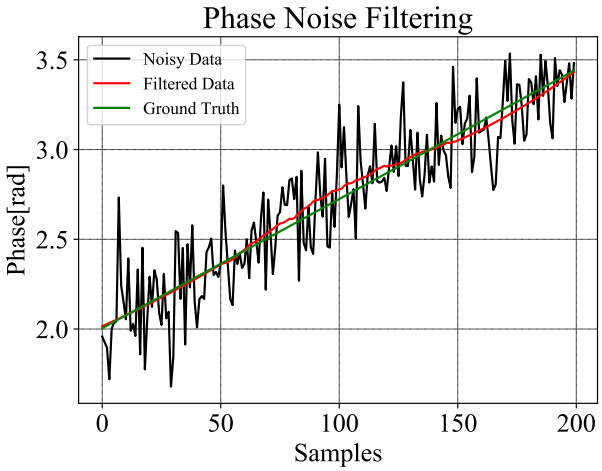

Fig. 4. Filtering out the noise of the phase measurements using a Savitzky–Golay filter.

phases measured from the same tag i at time instances t_{j-1}, t_j:

$$d\phi_j^i = \phi_j^i - \phi_{j-1}^i \tag{9}$$

By substituting filtered (8) in (9) the common unknown phase value ϕ_o^i is eliminated and $d\phi_j^i$ is given by:

$$\begin{aligned} d\phi_j^i &= \phi_{prop,j}^i + \phi_o^i - \phi_{prop,j-1}^i - \phi_o^i, \\ d\phi_j^i &= \phi_{prop,j}^i - \phi_{prop,j-1}^i \end{aligned} \tag{10}$$

Dividing (10) by $dt_j = t_j - t_{j-1}$ and substituting (5) in (10) results in the phase-ROC of tag i in time window $[t_{j-1}, t_j]$ which is expressed as:

$$\dot{\phi}_j^i = \frac{d\phi_j^i}{dt_j} = \frac{4\pi(d_j^i - d_{j-1}^i)/\lambda}{dt_j} \tag{11}$$

All rates are stored in a vector where each row depicts a period of time (i.e. a specific time window) and each column one of the surrounding tags. The ROC matrix $\mathbf{D}$ is formed as following:

$$\mathbf{D} = \begin{bmatrix} \dot{\phi}_1^1 & \dot{\phi}_1^2 & \dots & \dot{\phi}_1^N \\ \dot{\phi}_2^1 & \dots & \dots & \dots \\ \dots & \dots & \dots & \dots \\ \dot{\phi}_M^1 & \dots & \dots & \dot{\phi}_M^N \end{bmatrix}, \tag{12}$$

where N is the number of tags and M is the number of times $t_1, t_2, ..., t_M$ which form the time set at which the direction and location of the reader will be estimated.

B. Direction Estimation

To estimate the direction of the reader each time, the minimum of the ROCs of all tags is calculated:

$$\min \mathbf{D}[j,:] = \min([\dot{\phi}_j^1, ..., ..., \dot{\phi}_j^N]), \tag{13}$$

Fig. 5 shows a scenario where a reader moves across the dotted line from t_1 until t_2. Three surrounding tags are interrogated through the whole movement and phase data are gathered. The

reader is moving on a straight line towards tag #2. Using (11) the three phase rates of change are calculated:

$$\begin{aligned}\dot{\phi}_1^1 &= \frac{d\phi_1^1}{dt_1} = \frac{4\pi(d_2^1 - d_1^1)}{\lambda dt_1}\\ \dot{\phi}_1^2 &= \frac{d\phi_1^2}{dt_1} = \frac{4\pi(d_2^2 - d_1^2)}{\lambda dt_1}\\ \dot{\phi}_1^3 &= \frac{d\phi_1^3}{dt_1} = \frac{4\pi(d_2^3 - d_1^3)}{\lambda dt_1}\end{aligned} \tag{14}$$

The absolute difference of the radial distances between time instances t_1 and t_2 is greater for tag #2 which implies that $\dot{\phi}_1^2 < \dot{\phi}_1^3 < \dot{\phi}_1^1$. For tag #1 $\dot{\phi}_1^1 = 0$, since the radial distances are equal. Working vice versa, calculating the minimum ROC of sequential phase data in a time window gives us the reader's direction of movement.

Notice that even in a noise free environment the direction of movement can not be calculated precisely. If the reader is moving towards the area between two tags the direction of motion is determined from the tag that presents the minimum phase-ROC. The accuracy of the estimation depends on the number and density of the tags. The arrangement of the tags can change to meet the requirements of each application.

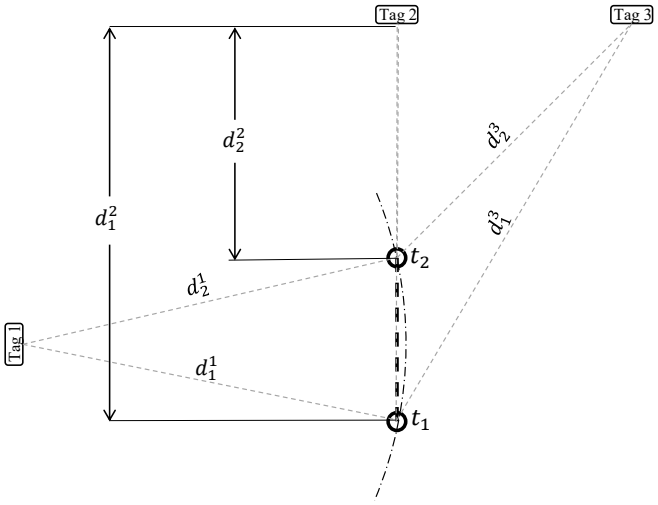

Fig. 5. A reader is moving towards tag #2 following the dotted line between t_1 and t_2. All three tags are interrogated by the reader along the trajectory followed.

C. Location Estimation

Equation (11) shows that the phase-ROC of tag i in a time window is proportional to the rate of change of the reader's position ($\Delta d/\Delta t$). This rate of change is in fact the radial velocity of the reader as observed from the corresponding tag i. Fig. 6 illustrates the trajectory followed by a reader from time instance t_{j-1} to t_j. The reader is constantly interrogating the four surrounding tags. Using (11) the radial speed vectors' magnitude $\|\vec{V_t^i}\|$ and angle $\angle\vec{V_t^i}$ are calculated and expressed by:

$$\|\vec{V_j^i}\| = \frac{(d_j^i - d_{j-1}^i)}{dt_j} = \frac{\lambda}{4\pi}\frac{d\phi_j^i}{dt_j}, \tag{15}$$

$$\angle\vec{V_j^i} = \angle(\mathbf{A}_{ant,j-1} - \mathbf{A}_{tag}^i), \tag{16}$$

where $\mathbf{A}_{ant,j-1}$ and $\mathbf{A}_{tag}^i$ are the positions of the antenna and tag i at time instant t_{j-1} correspondingly. The speed vector is calculated solving an optimization problem, formalised as [18]:

$$min\{(|V_j^i - \vec{V_j^i}|) \mid (\vec{V_j^1}, \angle\vec{V_j^1}), ..., (\vec{V_j^N}, \angle\vec{V_j^N})\}, \tag{17}$$

where $\vec{V_j^i}$ is the projection of speed vector $\overline{\mathbf{V}}_j$ at the direction of $\mathbf{A}_{ant,j-1}$ towards tag i. The accuracy of the estimated velocity depends on the placement of the tags and the effects of multipath and noise on the collected measurements.

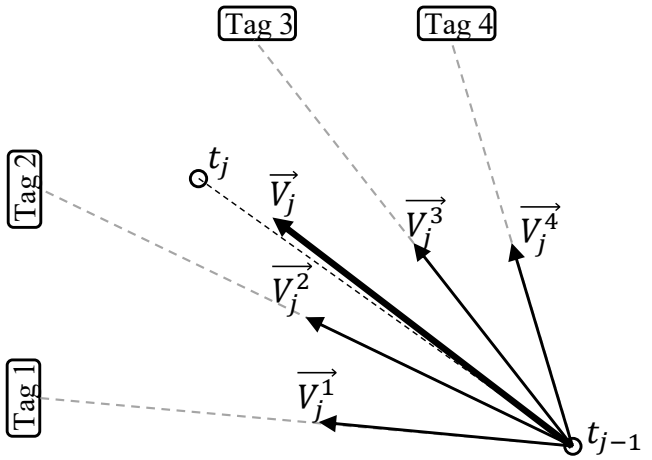

Fig. 6. Reader's speed approximation. The dotted line between time instance t_{j-1} and t_j denotes the trajectory followed by the reader. The radial velocity of the reader $\mathbf{V}_j$ is calculated by solving an optimization problem.

Estimating the dynamic state of a target can be decomposed in two processes: i) prediction and ii) update. The prediction stage or in robotics "the dead reckoning step" is concerned with the temporal development of the target state based on prior states, whereas the update stage is concerned with the adjustment of the anticipated state based on freshly acquired measurements. With this structure in mind, particle filters are deployed to address the tracking issue. By using a group of weighted particles, each of which represents a potential state with a given probability, particle filters (GAT) are able to solve the estimation problem. The set of particles is given by:

$$\left\{\mathbf{X}_j^n, w_j^n\right\}, n \in [1, N_p], \tag{18}$$

where $\mathbf{X}_j^n = \left\{x_j, y_j\right\}$ is the state vector and w_j^n is the significance weight of n-th particle at time instant t_j. The corresponding algorithm can be decomposed in the following 5 steps:

1) Initialization: A swarm of N_p particles, representing possible positions of the user, is generated. The particle set is uniformly sampled throughout the region of interest, exploiting Poisson disk sampling [29], since the tag locations are unknown at the initialization-step. Poisson disk sampling ensures that, all particles are separated by at least r, where r is a user-supplied density value. The weight of each particle is set to $1/N_p$. Knowledge of the search area's obstacles or antenna's characteristics could also be examined to lower the

number of necessary particles while keeping an equivalent particle density.

2) Dead reckoning, Prediction: The state of each particle changes according to its velocity vector calculated in (17). Only the three tags with the minimum phase-ROC (i.e. the tags that the user is moving towards to) are used for the calculation of the velocity vector and the new position is updated by:

$$\mathbf{X}_j^n = \mathbf{X}_{j-1}^n + \overline{\mathbf{V}}_j^n dt_j \tag{19}$$

3) Update Step: The weights are updated by summing the difference between the measured and the exact phase-ROCs $\dot{\phi}^i_{j,expected}$ assuming the user moves from position $\mathbf{X}^n_{j-1}$ to position $\mathbf{X}^n_j$ according to (19):

$$w_j^n = \left[\sum_{i=1}^{N} |\dot{\phi}^i_{j,expected} - \dot{\phi}^i_j|\right]^{-1}, \tag{20}$$

The weight of the particle, which location is closest to the reader's actual position would maximize (20). The weights are normalized, adding up to one, thus establishing a probability distribution.

4) Computing the State Estimate: The estimated position of the target time t_j is the weighted mean of the particle states:

$$\overline{\mathbf{X}}_j = \sum_{n=1}^{N_p} \vec{X}_j^n w_j^n \tag{21}$$

5) Particle Resampling: Particle filters suffer from the degeneracy problem. The procedure begins with evenly spaced out particles of equal weight. Only the particles that are close to the reader will have a meaningful weight after a few steps, at which point any particle that does not match the measurements will acquire an exceedingly low weight. The filter degenerates as less and fewer particles would now contribute significantly to the estimate of the state.

To counter this problem, a resampling step is implemented. The resampling method discards low-weighted particles and replaces them with new highly-weighted ones keeping the total number of particles constant. It accomplishes this by copying particles with relatively high weight. The noise introduced during the predict stage disperses the duplicates significantly. This yields a collection of points in which the vast majority of the particles appropriately represent the probability distribution. A majority of resampling methods have been developed that target on optimizing different characteristics (e.g. time, required memory, complexity etc).

In this paper stratified resampling was used to counter filter's degeneracy [30], [31]. The goal of stratified resampling is to choose among the particles fairly equally. It operates by splitting the whole amount into equal segments, and then generate N_p ordered random numbers using:

$$u_j = \frac{\tilde{u_j} + k}{N_p}, \tag{22}$$

where $k = 0, 1, 2, ..., N_p - 1$ and $\tilde{u_j} \sim \mathcal{U}(0, 1)$. the particles are then drawn independently in each of these subintervals, using the following condition which is based on the cumulative sum of normalized weights:

$$Q_j^{n-1} < u_j^k \leq Q_j^n, \tag{23}$$

where $Q_j^n = CumulativeSum[\{w^n_{norm,j}\}^N_{n=1}]$ Stratified resampling has a complexity of order $O(N)$ and guarantees that greater weights are resampled more frequently.

After resampling, the algorithm returns to step #2 and continues until the user has reached the target. The user is notified when the reader's to target distance is less than a predefined length.

III. Simulation

In this section the two parts of the method (i.e. direction and location estimation) are evaluated in simulated environments. Fig. 7 shows a top view of the simulations set-up. 20 tags were placed in a Γ arrangement and 3 trajectories were evaluated. Two distinct simulation modes were developed to evaluate

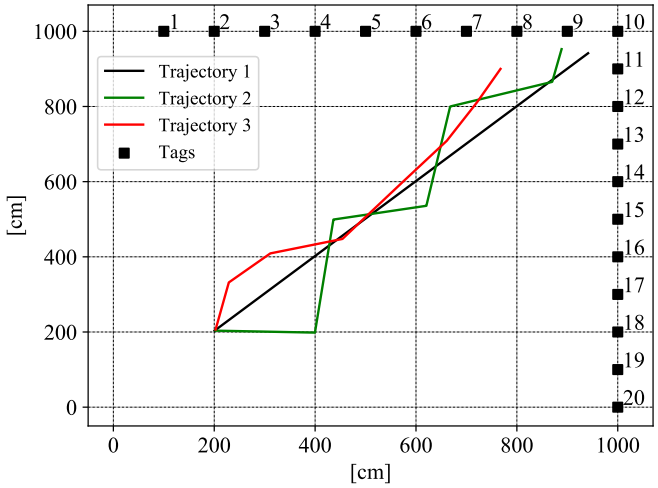

Fig. 7. Top view of the simulation setup and the simulated trajectories.

the accuracy and robustness of the algorithm. In the first mode the simulated user/reader follows a predefined trajectory and phase data were collected from all tags. In the second mode the user/reader is placed at an initial position and moves "freely" in the simulated environment, following the instructions derived by the destination estimation procedure of the algorithm. A random process was added to the calculated angle of rotation, to better imitate the movement and rotation of a human. Trajectories #1 and #2 were predefined and the first mode of the simulation evaluation was used, while trajectory #3 was generated using the second mode of the simulation evaluation. The direction and location estimation were evaluated separately and the results are presented in the following subsections.

A. Direction Estimation, Simulation

Initially the direction estimation is evaluated for trajectories #1 and #2. The user moves along the two paths and phase measurements are collected from the surrounding tags. Fig. 8 shows the unwrapped phase measurements and the calculated first phase-ROCs with respect to time for the first trajectory. The reader is moving towards tag #10 following a straight route and phase measurements collected from the 10-th tag present the maximum slope as shown in Fig. 8a. Due to

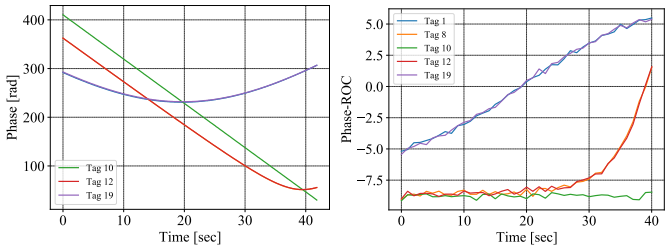

(a) Phase vs Time (b) Phase ROC vs Time

Fig. 8. Phase measurements and Phase-ROC vs time for trajectory #1

the symmetry of trajectory 1 the unwrapped phase curves of antipodal tags 8,12 and 1,19 in respect to the reader's position almost coincide. Both these characteristics are also apparent in Fig. 8b where Tag #10 presents the minimum phase-ROC and the phase-ROCs of the antipodal tags are similar through the whole path followed. In addition the phase-ROC is getting larger as the user is moving away from a tag.

The efficiency of the direction estimation procedure exploiting phase-ROC is demonstrated in Fig. 9 where the phase-ROCs over time for the second trajectory are plotted. The user is changing the direction of motion by moving in a zig-zag pattern. The alternating direction is depicted in the minimum phase-ROCs of Fig. 9. The id of the tag presenting the minimum phase-ROC in each time window is annotated.

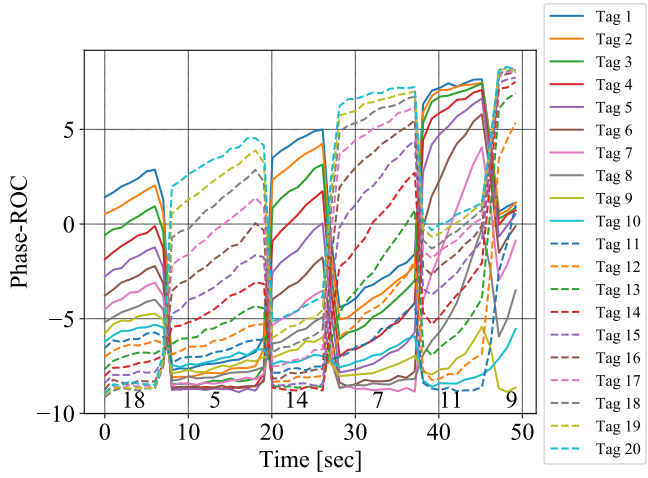

Fig. 9. Phase-ROC measurements over time for trajectory #2

After ensuring that the direction of the reader/user can be extracted from the minimum phase-ROC measurements, the direction estimation method was tested in the second simulation mode. The initial orientation of the user is random and changes based on the calculations of the direction estimation algorithm in order to guide one to the target tag (i.e. Tag #8). To better imitate a human's motion a random process was added to the user's rotation. In Fig. 10 the trajectory created by the autonomous motion of the user is plotted along with the algorithm's instructions annotated at the positions that they were given. It is shown that the user is successfully guided to the target tag.

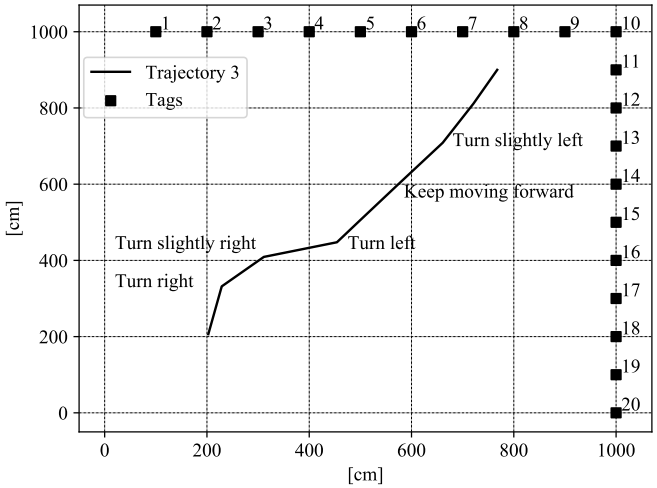

Fig. 10. Trajectory created by the autonomous motion of the user during simulation.

B. Location Estimation, Simulation

Location estimation is evaluated in all three trajectories. Fig. 11 illustrates the steps of the particle filter algorithm for trajectory #1. At first a swarm of N_p particles is initialized using Poisson disk sampling with a separation value $r = 50\ cm$ as shown in Fig. 11a.

After a time window of 1 second, the phase measurements collected from all 20 tags are processed and the speed $\overline{\mathbf{V}}_j^n$ estimated from the radial velocity vectors of the three tags with the smallest phase-ROCs is calculated for each particle using (17). Substituting $\overline{\mathbf{V}}_j^n$ in (19) a new position for every particle is calculated. The dead-reckoning process is presented in Fig. 11b where the speed vector is plotted as an arrow starting from the initial position of each particle and ending in each particle's new position after dead-reckoning.

In the third step the weights of all particles are updated by comparing the measured and theoretical phase-ROCs collected from all tags. The updated particles are presented in Fig. 11c, where particles with larger weights are drawn with hotter colors. The highly weighted particles are the ones that their "assumed" position agrees more with the actual. The state estimate is calculated using (21) and is shown in the same figure with an "x" mark.

To counter the particle degeneracy problem a resampling step is vital. The particles are practically regenerated in new positions closer to the positions of the highly weighted particles. In Fig. 11d the number of the particles is the same as the previous step but instead of being randomly scattered in the search area they are gathered around the positions of the particles with the largest weights.

After the resampling step, the location estimation algorithm returns to step #2 and continues until the end of the simulated path. The initial assumptions of the localized pose, present large errors as the particle locations spread across the search area. As the user moves further the particles converge to an estimate closer to the actual position. This property is shown in Fig. 11e, where the algorithm has completed 9 iterations for 9 time windows and has "locked" the actual position.

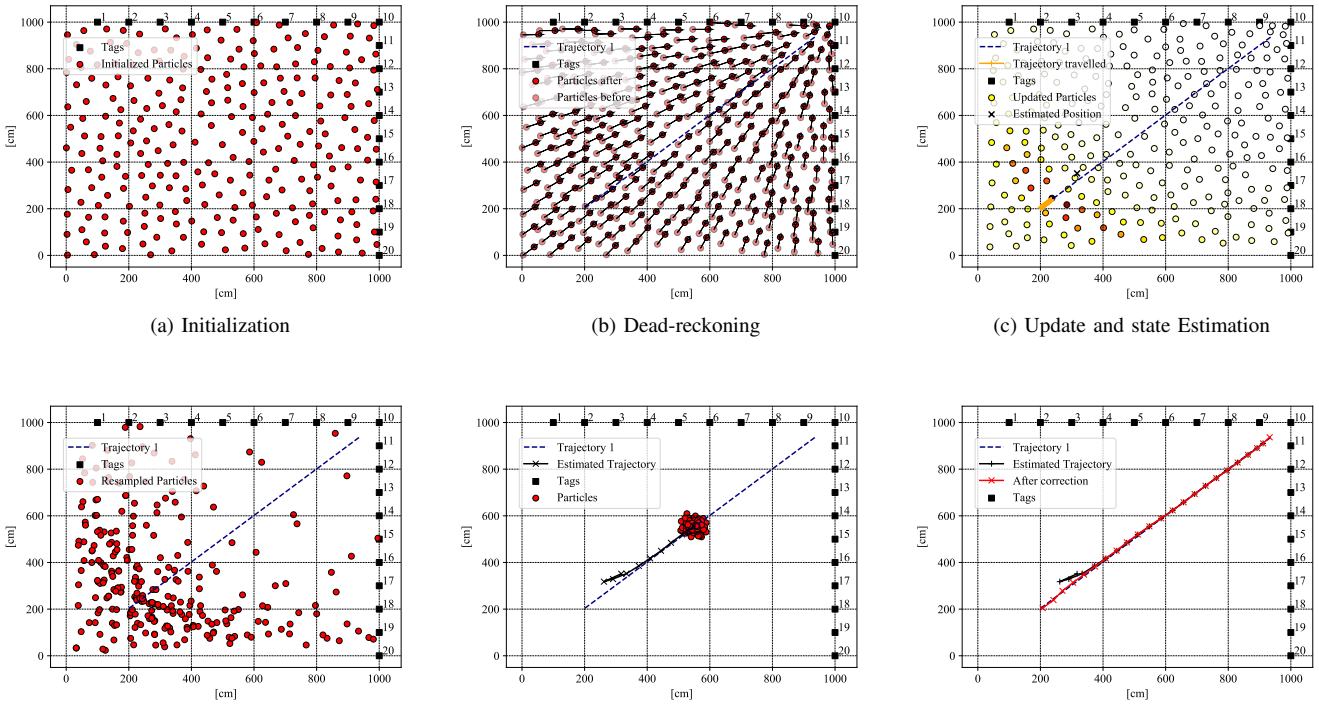

(a) Initialization (b) Dead-reckoning (c) Update and state Estimation

(d) Resampling (e) Particles and estimates after 9 steps (f) Estimated trajectory vs ground trouth

Fig. 11. Graphical representation of the localization part of the algorithm in a simulated environment.

The complete estimation of the trajectory is illustrated in Fig. 11f. Due to the dispersion of the particles at the first steps of the algorithm the estimation accuracy of the trajectory is poor. To smooth and fix the trajectory a "re-estimation" step could be integrated. The "re-estimation" process starts at a time when the particles have converged to a position and created a cluster around a central position c_j. The particles are presumed to have converged when:

$$\frac{1}{N_p}\sum_{n=1}^{N_p}||\vec{X}_j^n - c_j||_2 \leq d_p, \tag{24}$$

where parameter d_p has been set to 20 cm. The estimated position of the target at this time instance is considered the initial position. Simple dead reckoning is exploited to estimate the previous positions. In this case the estimated position at time step #7 is picked and dead reckoned 7 times using the opposite resultant speed vector calculated at each previous step. The corrected trajectory is plotted in Fig. 11f with a red line.

Since random processes are involved in both the initialization and the resampling step the estimation accuracy of the algorithm need to be calculated multiple times. The algorithm was executed 50 times for each trajectory and the error was calculated for each run. To determine the error per run, the differences between the estimated and "actual" positions at each time window are summed and divided by M (i.e. the total number of time steps):

$$Error = \frac{\sum_{j=1}^{M}||\overline{\mathbf{X}}_{j\_est} - \overline{\mathbf{X}}_{j\_real}||_2}{M} \tag{25}$$

TABLE I
LOCATION ESTIMATION ALGORITHM SIMULATION ERROR

Paths	Distance (cm)	Mean Error(cm)	Std (cm)
Trajectory 1	1045.52	6.55	0.95
Trajectory 2	1257.89	17.67	3.2
Trajectory 3	941.19	9.35	2.68

The mean absolute value of all errors and standard deviations for all runs along with the distance travelled per trajectory are presented in Table I.

1) Number of particles: The algorithm's efficiency in terms of time and accuracy depends on the number of particles N_p. The number of particles is selected based on the desired separation value r , which denotes the minimum distance between samples during the initialization of the filter, using Poisson disk sampling. The total number of particles decreases as the sampling distance increases. As a result, there is a trade-off between computational expense and estimate variance. A study on the effect of r for trajectory #2 was conducted in order to select a suitable separation value r for the filter. The search area is considered $10x10m^2$, which is reasonable, given the read-range of passive UHF RFID technology. For each r, the location estimation algorithm was repeated 50 times. The "mean" results are summarized in Table II. The mean N_p value over 50 iterations of the method for each r is displayed in the second column.The third and fourth columns provide the mean absolute value of all errors (determined using (25)) and standard deviations for all runs for various r, respectively. As

TABLE II
NUMBER OF PARTICLES ANALYSIS

r	N_p	Mean Error	Std	"Locked" Step	Time
10	6212.88	18.68	1.958	3	9.441
20	1569.24	18.31	2.65	4	0.956
40	399.24	18.61	2.87	5	0.154
60	180.24	19.34	4.52	5	0.064
80	104.0	20.88	6.43	6	0.036
100	66.88	24.99	14.92	7	0.022
120	48.26	33.99	21.64	8	0.017
140	35.62	41.47	30.03	10	0.013
160	27.68	47.81	33.40	10	0.0106
180	22.18	54.42	39.16	11	0.009
200	18.08	69.58	47.13	12	0.007

TABLE III
MULTIPATH ANALYSIS

A	Mean Error (cm)	Standard deviation (cm)	"Locked" Step
0.0	17.85	3.46	4
0.1	18.75	7.62	4
0.2	18.69	6.6	6
0.3	22.08	8.93	7
0.4	24.31	11.12	8
0.5	26.08	10.22	8
0.6	28.65	12.33	9
0.7	30.69	11.00	9
0.8	29.89	11.56	10
0.9	32.31	11.76	11
1.0	36.67	13.53	11

N_p increases, mean error and standard deviation are improved. The fifth column shows at which step/iteration the algorithm "locked" to the position of the user most of the times. The locked state is the step when the distance between the real and the estimated position is less than 25 cm. When r is large less particles are uniformly scattered around the search area, and only a handful of particles are near the user's real position having an appreciable weight, leading to a degenerated filter. Although resampling solves the issue in all cases, more steps are needed. The sixth column refers to the average time per iteration (step). When the number of particles increases, the computing cost increases significantly, making the time required for each iteration prohibitive for real-time applicability of the method. Assuming maximum estimation time in the order of 100 ms and a search space of 100 m^2, r should be set to 50 cm, "locking" the user's position at the 5th iteration.

2) Multipath: The effect of multipath on the algorithm's performance is investigated. Phase-data are generated, using (2) for increasing values of A in order to simulate different levels of multipath-rich environments. The results are presented in Table III. The algorithm managed to keep a mean error less than 40 cm even for the highest values of A ($A = 1$ implies that the magnitude of the multiply reflected contributions equal that of the LOS field). The algorithm needs more iterations to "lock" for increased fading. Jittering of particles eventually compensate multipath effects. The robustness and performance of the method in real scenarios is experimentally evaluated in section IV in real environments.

IV. EXPERIMENTS

The experiments were carried out in the School of Electrical and Computer Engineering of the Aristotle University of Thessaloniki. A robot replaces the "human", in order to collect precise estimations of its trace with respect to time and compare with the proposed method. The robot is equipped with an Impinj R420 reader ($P_{transmit} = 30dBm$) and a UHF-RFID antenna manufactured by RFMAX (R8658-LPV-SSF).

The antenna used is circularly polarized directional antenna with a gain of 8.5 dBic. A directional antenna is used since this type of antennas are commonly found in handheld readers. An omnidirectional antenna along the horizontal plane would have enhanced the algorithm because, in that case, the reader would have been able to measure the phase from tags in the left/right and back directions, providing useful information to the filter (positive phase-ROC from such tags, hence greater differences in the weighting function). As "weights" would vary more in this situation, the filters would have locked the target sooner. The disadvantage is that the read-range would have been constrained and the user might have been "walking" in bigger regions without knowledge of the position.

The robot uses a lidar sensor in conjunction with odometry sensors and Kalman filtering to perform Simultaneous Localization and Mapping (SLAM) and estimate its pose at cm-accuracy. This position is considered the "ground truth" of the experiment. The set up of the experiments can be seen in Fig. 12. Alien ALN-9740 "Squiggle" RFID tags with "Higgs–4" IC (-19 dBm sensitivity) are placed at a Γ configuration on top of wooden desks in a multipath-rich lab at known locations. For each experiment the robot was positioned at a different starting position and a tag id was given as the target. The robot started moving and traversed a trajectory according to the instructions given by the direction estimation part of the algorithm. When the robot approached the designated goal, the operator of the remote controller stopped the robot's progress. Fig. 13 shows a top view of the experiments' setup along with the different trajectories followed by the robot along different experiments. The distance between each tag was 30 cm for configuration A and 50 cm for configuration B, leading to a total number of 22 and 14 tags, respectively. The search area for the location estimation algorithm was a $3.5x2.5m^2$ space in front of the tags.

A. Direction Estimation

The target tag for each experiment along with the speed and the total distance travelled by the robot are presented in table IV . Comparing the last position of each trajectory and the target tag of the corresponding experiment, it is found that the direction estimation algorithm has successfully guided the robot to the desired target in all cases (100% success). To further investigate the accuracy of the algorithm

Fig. 12. The experiments' set up includes 22 tags, placed at a Γ configuration on top of desks in a multipath rich lab.

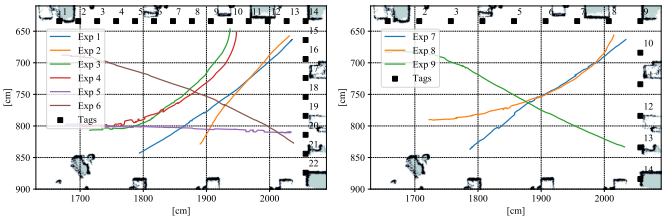

(a) Configuration A (b) Configuration B

Fig. 13. Top view of the trajectories and the experiments' setup for both tag configurations.

on determining the direction of the robot at each time window the pose of the robot (i.e. x, y, θ) along with the decisions made by the direction estimation algorithm at each time window are saved for each experiment. The direction estimations are compared with the real θ of the robot at each time window. If the robot's real direction resembles with either the direction of the tag that the robot is moving towards to or its closest neighbor then the algorithm is presumed to have made a right estimation. The percentages of the right estimations per experiment are presented in Table IV.

B. Location Estimation and Comparison to Prior Art

During the experiments, the postures of the moving robot were estimated by a SLAM algorithm at cm accuracy. The location estimation part of the method (as described in sections II-C and III-B) is tested for all 9 trajectories. The mean error (calculated using (25)) and standard deviation of "GuideAndTrack" are compared to "Tagoram" in Table V. "Tagoram" is designed to perform object localization and tracking, using fixed antennas and moving tags achieving real time estimations with high accuracy. The reason "Tagoram" was chosen for comparison is that *i)* it is the only technique that can work under the same assumptions i.e. a reader and RFID tags, *ii)* is a well established method in the prior art, and *iii)* exploits phase-ROC. The mean error was small in all experiments for "GuideAndTrack", while "Tagoram" suffered larger errors in some experiments, which will be commented in the following paragraphs.

TABLE IV
DIRECTION ESTIMATION ALGORITHM ERROR

Exp	Target Id	Speed (cm/s)	Distance (cm)	Percentage (%)
1	14	15	312.39	95.23
2	14	22.5	223.34	100
3	10	15	309.92	95.23
4	10	22.5	361.47	91
5	20	15	404.69	100
6	21	15	412.07	100
7	9	15	317.58	94.11
8	8	15	354.82	100
9	13	22.5	420.85	100

TABLE V
GUIDEANDTRACK VS TAGORAM, LOCATION ESTIMATION ERROR

Exp	Target	Speed	Mean Error (cm)		Std (cm)	
			GAT	Tagoram	**GAT**	Tagoram
1	14	15	**24.75**	35.09	**10.45**	2.11
2	14	22.5	**20.86**	29.92	**4.89**	2.04
3	10	15	**20.10**	38.42	**6.89**	4.5
4	10	22.5	**10.81**	28.64	**4.56**	3.4
5	20	15	**21.45**	82.81	**9.59**	3.39
6	21	15	**17.34**	160.81	**5.97**	7.25
7	9	15	**15.68**	151.28	**9.17**	11.68
8	8	15	**27.22**	137.07	**8.59**	8.97
9	13	22.5	**29.5**	25.75	**11.80**	7.41

A characteristic result of the complete estimation of the trajectory by the proposed method is illustrated in Fig. 14 (experiment #4). The ground truth path and the estimated trajectory are plotted with blue and black lines respectively. The corrected trajectory after the "re-estimation" process is shown with red color. Notice that the "forward-only" estimated trajectory (shown in black) fails to lock the position during the initial 6 steps of the robot, as the particles "search" the entire area; as soon as the position is found, the algorithm never misses the robot again in the remaining path. Those initial 6 steps are corrected during the "re-estimation" process (shown in red), where the past measurements are traced backwards. The method performed similarly in all experiments.

To apply "Tagoram" we have reversed the assumption of a single moving tag measured by multiple readers at known positions, namely "a single moving reader measures multiple tags at known positions". According to "Tagoram", data-derived tracks are computed and a hologram is formed,

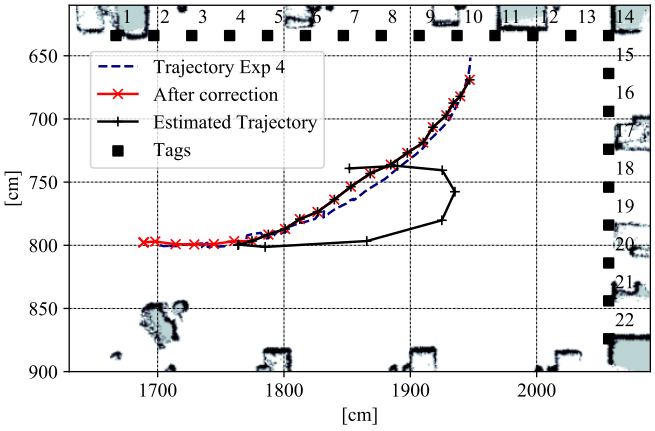

Fig. 14. The estimated trajectory vs the ground truth for experiment 4.

representing the starting location of the time frame. Initially, we applied "Tagoram" taking into account all tags. The estimation-errors were large, because the tags were not placed uniformly around the room (in all directions, surrounding the reader); consequently forcing the velocity vectors towards a given area of the room. It was found that "Tagoram" was improved by considering the velocity vector from the three tags that were closer to the direction of motion, i.e. the three measured smallest phase-ROCs. In general, "Tagoram" failed to achieve high accuracy, unless the initial position matched the grid.

Table VI highlights each method's performance in terms of accuracy vs computation time. Tagoram's computation time depends on the density of the grid, while GAT's computation time depends on the number of particles. The execution time in Table VI refers to the average time per iteration (step) from all experiments. The proposed technique achieves the highest accuracy while incurring the least computing cost. It takes only 0.1 seconds to update the position of the user with 400 particles. Moreover, GAT tracked the target with a mean error less than 33 cm even when considering only 100 particles, delivering each estimation after 20 ms. On the contrary, even when considering a dense grid spacing of 2.5 cm, "Tagoram" suffered from a mean error of more than 70 cm while taking 11.5 seconds to update the position. Analytical results from all experiments, assuming the 2.5 cm grid are shown in Table V.

Fig. 15 shows the estimated trajectories for both "Tagoram" and "GAT" versus the ground truth. Tagoram performs well on estimating the track exploiting the velocity vectors from the tags. When the initial estimated position is close to the real one the mean error of Tagoram is comparable to GAT's as shown in Fig. 15a. On the other hand if the Tagoram fails on accurately estimating the initial position of the reader the total error worsens. We expect the performance of both methods to be comparable when tags surround the area of movement of the user, since under such circumstance, the velocity vector and the initial position would have been properly estimated by "Tagoram".

TABLE VI
GUIDEANDTRACK VS TAGORAM, LOCALIZATION ERROR AND EXECUTION TIME PER ITERATION

Method	Mean Error (cm)	Execution Time (s)
GAT (N_p=2000)	**28.45**	**1.1**
Tagoram (2.5 cm grid)	76.65	11.54
GAT (N_p=400)	**20.9**	**0.11**
Tagoram (8.5 cm grid)	87.33	2.36
GAT (N_p=100)	**32.80**	**0.02**
Tagoram (15 cm grid)	98.66	1.5

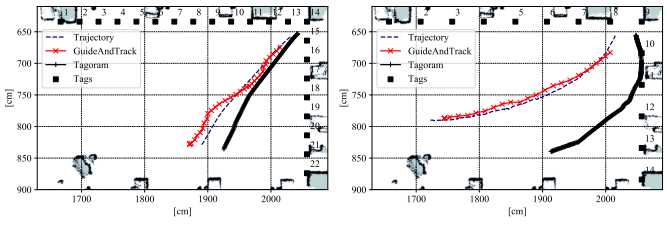

(a) Experiment 2 (b) Experiment 8

Fig. 15. Tagoram's estimated trajectories for experiments 2 and 8

C. Experiments with a Portable Reader

Experiments with a prototype portable UHF-RFID reader (shown in Fig. 16 were conducted to verify the method's accuracy in a real-world setting. In contrast to the robot's smooth motion, the human's motion is characterized by fluctuations in the velocity vector along all axes, including height displacements during the steps. The experiments were conducted in a $4.5x3.5m^2$ area of the Campus. The portable RFID reader consists of the following components:

- ThingMagic Sargas 2-Port UHF RFID Reader
- Laird Technologies PER86506 Antenna (Gain 6 dBic)
- Raspberry pi 4
- Touch screen
- Power supply system
- 3D printed casing

An application has been developed that guides the user to the selected target tag, while estimating his pose. Fig. 17 shows the user interface of the application. The user selects the desired target and presses the "start reading" button to initialize "GAT". The application guides the user towards the right direction by turning the appropriate arrows green. The location estimation algorithm is executed in parallel to estimate the user's position. The estimated coordinates in the map and the distance from the selected target are printed on the top of the screen.

Fig. 18 shows the arrangement of the experiments. Ten cardboard boxes with 10 Alien ALN-9740 "Squiggle" RFID tags with "Higgs-4" ICs (-19 dBm sensitivity) are set on top of wooden shelves. The distance between the tags was 45 cm.

ArUco markers are utilized to determine the actual position of the reader or person [32]. As seen in Fig. 16b, such a square marker is attached on the front of the portable reader. The reader's position is determined during the tests by a laptop equipped with a camera detecting the position of the marker

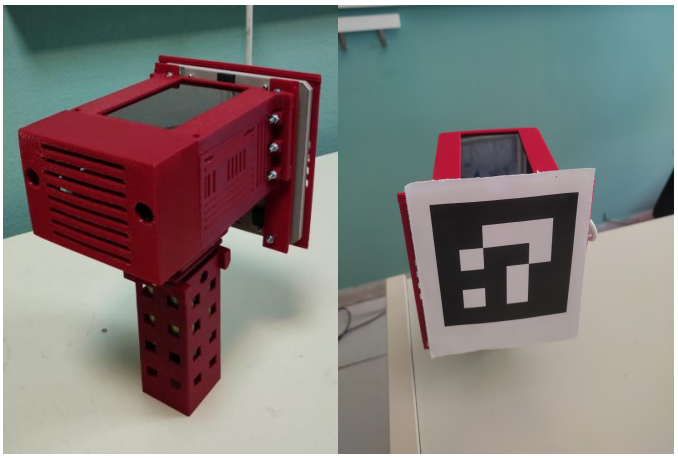

(a) Back View (b) Front View

Fig. 16. The prototype portable UHF-RFID reader.

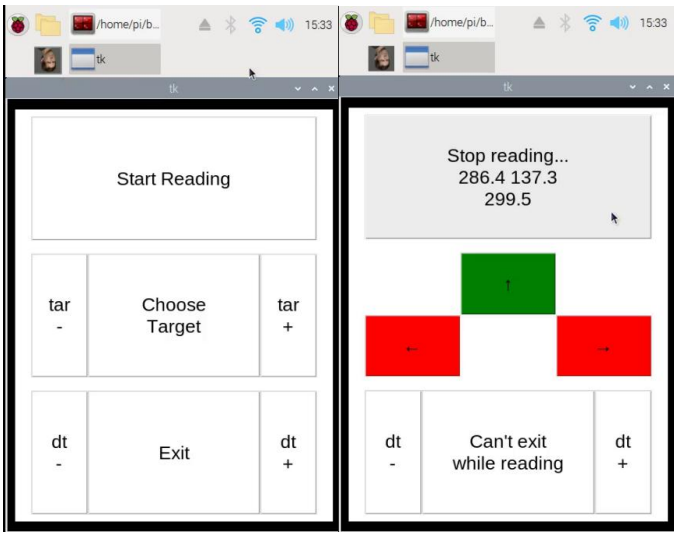

(a) Initial View (b) Running View

Fig. 17. The application on the touch screen of the reader.

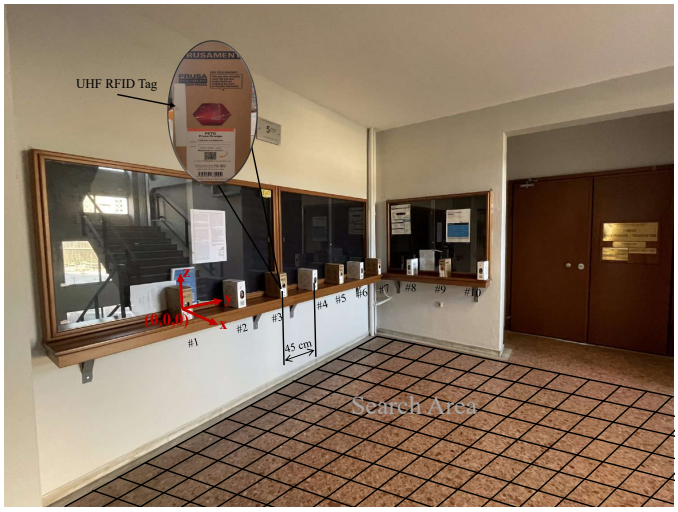

Fig. 18. The setup of the experiments with the portable reader.

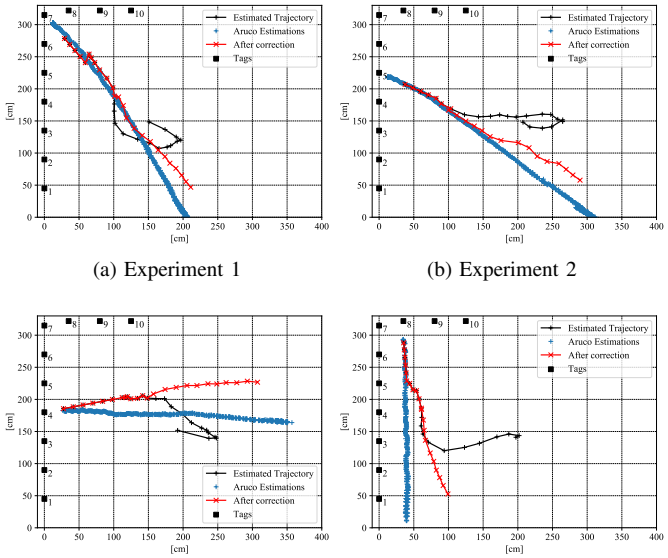

(a) Experiment 1 (b) Experiment 2

(c) Experiment 3 (d) Experiment 4

Fig. 19. Estimated trajectory vs ground truth for all experiments.

with respect to the camera's pose in the map. This visual estimation is considered to be the ground truth of this set of experiments.

The user selected four different targets from four different initial positions. "GAT" successfully guided the user to the desired target in all cases and gave an estimation of the reader's position every second enabling the user to know when the target was reached. GAT's estimated trajectories before and after correction are shown in Fig. 19 with black and red color respectively. In all cases, "GAT" successfully guided and "locked" the position of the user after a few iterations, once again verifying its robustness for the non-smooth motion of a human.

V. Discussion

This paper presents a prototype RFID-based system for directing a user to a specific tag, while estimating the user's pose. A portable reader that can identify adjacent tags and gather phase measurements is given to the user. Estimates of the user's direction and position are continuously updated. Regardless of the user's pace or distance traveled, experimental results verified accurate performance. The key for the success of "GuideAndTrack" is the fact that it is based on estimating the Rate Of Change of phase; as a consequence, there is no need for phase unwrapping of measurements during the entire human's path but only during a given time-slot. The necessary estimation-time is small enough to be exploited in real-time applications. Notice that estimation of the user's pose is independent from the guidance-process; the user's pose is identified and tracked even if one roams freely in any area with RFID tags at known positions.

One interesting perspective of the proposed method is its potential application in guiding blind. The specific problem has been considered as an application in the Archaeological Museum of Thessaloniki, where RFID-tags had already been

attached to the exhibits. So the set-up is convenient, as the central area of each exhibition-room is empty and the exhibits are next to the surrounding walls. The basic idea is: If 1) you are "confident" that you can track the position of someone, i.e by the proposed method, 2) you know the map of the environment and 3) you know where one wants to go in the map, then you would guide one from the proper path (not necessarily a straight path), avoiding possible firm-obstacles. All these conditions are met in the museum. However, the method is not suitable by itself for avoidance of moving obstacles.

Another interesting perspective is to exploit the proposed method for human-guidance along "RFID-paths", created by sequences of RFID tags; thus incorporating a new idea of RFID-lanes.

REFERENCES

[1] C. Wu, F. Zhang, B. Wang and K. J. R. Liu, "EasiTrack: Decimeter-Level Indoor Tracking With Graph-Based Particle Filtering," in IEEE Internet of Things Journal, vol. 7, no. 3, pp. 2397-2411, March 2020, doi: 10.1109/JIOT.2019.2958040.

[2] S. Depatla and Y. Mostofi, "Passive Crowd Speed Estimation in Adjacent Regions With Minimal WiFi Sensing," in IEEE Transactions on Mobile Computing, vol. 19, no. 10, pp. 2429-2444, 1 Oct. 2020, doi: 10.1109/TMC.2019.2924629.

[3] A. Nakib, B. Daachi, M. Dakkak and P. Siarry, "Mobile Tracking Based on Fractional Integration," in IEEE Transactions on Mobile Computing, vol. 13, no. 10, pp. 2306-2319, Oct. 2014, doi: 10.1109/TMC.2013.37.

[4] S. Siachalou, A. Bletsas, J. Sahalos and A. G. Dimitriou, "RSSI-based maximum likelihood localization of passive RFID tags using a mobile cart," 2016 IEEE Wireless Power Transfer Conference (WPTC), 2016, pp. 1-4, doi: 10.1109/WPT.2016.7498847.

[5] D. Joho, C. Plagemann and W. Burgard, "Modeling RFID signal strength and tag detection for localization and mapping," 2009 IEEE International Conference on Robotics and Automation, 2009, pp. 3160-3165, doi: 10.1109/ROBOT.2009.5152372.

[6] J. Zhang, Y. Lyu, J. Patton, S. C. G. Periaswamy and T. Roppel, "BFVP: A Probabilistic UHF RFID Tag Localization Algorithm Using Bayesian Filter and a Variable Power RFID Model," in IEEE Transactions on Industrial Electronics, vol. 65, no. 10, pp. 8250-8259, Oct. 2018, doi: 10.1109/TIE.2018.2803720.

[7] A. Motroni, P. Nepa, P. Tripicchio and M. Unetti, "A Multi-Antenna SAR-based method for UHF RFID Tag Localization via UGV," 2018 IEEE International Conference on RFID Technology & Application (RFID-TA), 2018, pp. 1-6, doi: 10.1109/RFID-TA.2018.8552780.

[8] A. Tzitzis et al., "Localization of RFID Tags by a Moving Robot, via Phase Unwrapping and Non-Linear Optimization," in IEEE Journal of Radio Frequency Identification, vol. 3, no. 4, pp. 216-226, Dec. 2019, doi: 10.1109/JRFID.2019.2936969.

[9] A. Tzitzis, A. Raptopoulos Chatzistefanou, T. V. Yioultsis and A. G. Dimitriou, "A Real-Time Multi-Antenna SAR-Based Method for 3D Localization of RFID Tags by a Moving Robot," in IEEE Journal of Radio Frequency Identification, vol. 5, no. 2, pp. 207-221, June 2021, doi: 10.1109/JRFID.2021.3070409.

[10] A. Tzitzis, A. Malama, V. Drakaki, A. Bletsas, T. V. Yioultsis and A. G. Dimitriou, "Real-Time, Robot-Based, 3D Localization of RFID Tags, by Transforming Phase Measurements to a Linear Optimization Problem," in IEEE Journal of Radio Frequency Identification, vol. 6, pp. 439-455, 2022, doi: 10.1109/JRFID.2021.3103393.

[11] A. Motroni et al., "SAR-Based Indoor Localization of UHF-RFID Tags via Mobile Robot," 2018 International Conference on Indoor Positioning and Indoor Navigation (IPIN), 2018, pp. 1-8, doi: 10.1109/IPIN.2018.8533847.

[12] L. Shangguan and K. Jamieson, "The Design and Implementation of a Mobile RFID Tag Sorting Robot", in Proceedings of the 14th Annual International Conference on Mobile Systems, Applications, and Services (MobiSys '16), Association for Computing Machinery, New York, NY, USA, 31–42, 2016, doi:10.1145/2906388.2906417.

[13] Xin Li, Y. Zhang and M. G. Amin, "Multifrequency-based range estimation of RFID Tags," 2009 IEEE International Conference on RFID, 2009, pp. 147-154, doi: 10.1109/RFID.2009.4911199.

[14] A. R. Chatzistefanou, A. Tzitzis, S. Megalou, G. Sergiadis and A. G. Dimitriou, "Target Localization by Mobile Handheld UHF RFID Reader and IMU," in IEEE Journal of Radio Frequency Identification, vol. 6, pp. 426-438, 2022, doi: 10.1109/JRFID.2022.3147539.

[15] K. Singh et al., "Localization of Life Safety Vests in an Aircraft Using Backscattering RFID Communication," in IEEE Journal of Radio Frequency Identification, vol. 4, no. 3, pp. 234-245, Sept. 2020, doi: 10.1109/JRFID.2020.3005248.

[16] E. DiGiampaolo and F. Martinelli, "Range and Bearing Estimation of an UHF-RFID Tag Using the Phase of the Backscattered Signal," in IEEE Journal of Radio Frequency Identification, vol. 4, no. 4, pp. 332-342, Dec. 2020, doi: 10.1109/JRFID.2020.3016168.

[17] A. Parr, R. Miesen, F. Kirsch and M. Vossiek, "A novel method for UHF RFID tag tracking based on acceleration data," 2012 IEEE International Conference on RFID (RFID), 2012, pp. 110-115, doi: 10.1109/RFID.2012.6193037.

[18] L. Yang, Y. Chen, X. Li, C. Xiao and Y. Liu, "Tagoram: Real-time tracking of mobile RFID tags to high precision using COTS devices," Proceedings of the Annual International Conference on Mobile Computing and Networking, MOBICOM, 2014, doi: 10.1145/2639108.2639111.

[19] R. Mautz, "Indoor positioning technologies," Doctoral dissertation, Dept. Civil, Environ. Geomatic Eng., Inst. Geodesy Photogramm., ETH Zurich, Zurich, Switzerland, 2012

[20] P. Levchev, M. N. Krishnan, C. Yu, J. Menke and A. Zakhor, "Simultaneous fingerprinting and mapping for multimodal image and WiFi indoor positioning," 2014 International Conference on Indoor Positioning and Indoor Navigation (IPIN), 2014, pp. 442-450, doi: 10.1109/IPIN.2014.7275515.

[21] G. Gerstweiler, E. Vonach, and H. Kaufmann, "HyMoTrack: A Mobile AR Navigation System for Complex Indoor Environments," Sensors, vol. 16, no. 1, p. 17, Dec. 2015, doi: 10.3390/s16010017.

[22] U. Rehman, and S. Cao, "Augmented-Reality-Based Indoor Navigation: A Comparative Analysis of Handheld Devices Versus Google Glass," in IEEE Transactions on Human-Machine Systems, vol. 47, no. 1, pp. 140-151, Feb. 2017, doi: 10.1109/THMS.2016.2620106.

[23] A. Mulloni, H. Seichter, and D. Schmalstieg, "Handheld augmented reality indoor navigation with activity-based instructions," in Proceedings of the 13th International Conference on Human Computer Interaction with Mobile Devices and Services (MobileHCI '11), Association for Computing Machinery, New York, NY, USA, 211–220., Aug. 2011, doi: 10.1145/2037373.2037406

[24] Skulimowski, P., Owczarek, M., Radecki, A. et al, "Interactive sonification of U-depth images in a navigation aid for the visually impaired," Journal on Multimodal User Interfaces, volume 13, 219–230 (2019), doi: 10.1007/s12193-018-0281-3.

[25] J. Wang, E. Liu, Y. Geng, X. Qu and R. Wang, "A Survey of 17 Indoor Travel Assistance Systems for Blind and Visually Impaired People," in IEEE Transactions on Human-Machine Systems, vol. 52, no. 1, pp. 134-148, Feb. 2022, doi: 10.1109/THMS.2021.3121645.

[26] W. Hu, K. Wang, H. Chen, R. Cheng, and K. Yang, "An indoor positioning framework based on panoramic visual odometry for visually impaired people," Meas. Sci. Technol., vol. 31, no. 1, 2019, Art. no. 014006, doi: 10.1088/1361-6501/ab40d9

[27] S. A. Cheraghi, V. Namboodiri and L. Walker, "GuideBeacon: Beacon-based indoor wayfinding for the blind, visually impaired, and disoriented," 2017 IEEE International Conference on Pervasive Computing and Communications (PerCom), 2017, pp. 121-130, doi: 10.1109/PERCOM.2017.7917858.

[28] P. V. Nikitin, R. Martinez, S. Ramamurthy, H. Leland, G. Spiess and K. V. S. Rao, "Phase based spatial identification of UHF RFID tags," 2010 IEEE International Conference on RFID (IEEE RFID 2010), 2010, pp. 102-109, doi: 10.1109/RFID.2010.5467253.

[29] R. Bridson, "Fast Poisson disk sampling in arbitrary dimensions," in ACM SIGGRAPH 2007 sketches (SIGGRAPH '07), Association for Computing Machinery, New York, NY, USA, 22–es. https://doi.org/10.1145/1278780.1278807

[30] T. Li, M. Bolic and P. M. Djuric, "Resampling Methods for Particle Filtering: Classification, implementation, and strategies," in IEEE Signal Processing Magazine, vol. 32, no. 3, pp. 70-86, May 2015, doi: 10.1109/MSP.2014.2330626.

[31] J. D. Hol, T. B. Schon and F. Gustafsson, "On Resampling Algorithms for Particle Filters," 2006 IEEE Nonlinear Statistical Signal Processing Workshop, Cambridge, UK, 2006, pp. 79-82, doi: 10.1109/NSSPW.2006.4378824.

[32] S. Garrido-Jurado, R. Muñoz-Salinas, F. J. Madrid-Cuevas and M. J. Marín-Jiménez, "Automatic generation and detection of highly reliable

fiducial markers under occlusion", Pattern Recognition vol. 47, 6 June 2014, pp. 2280-2292. doi: 10.1016/j.patcog.2014.01.005